Defect-induced faceted blue phosphorene nanotubes

Yierpan Aierken,[*] Ortwin Leenaerts,[†] and François M. Peeters[‡]
Department of Physics, University of Antwerp, Groenenborgerlaan 171, B-2020 Antwerpen, Belgium
(Received 26 June 2015; published 11 September 2015)

The properties of a new class of phosphorene nanotubes (PNT) are investigated by performing first-principles calculations. We demonstrate that it is advantageous to use blue phosphorene in order to make small nanotubes and propose a way to create low-energy PNTs by the inclusion of defect lines. Five different types of defect lines are investigated and incorporated in various combinations. The resulting defect-induced faceted PNTs have negligible bending stresses which leads to a reduction in the formation energy with respect to round PNTs. Our armchair faceted PNTs have similar formation energies than the recently proposed multiphase faceted PNTs, but they have a larger variety of possible structures. Our zigzag faceted PNTs have lower formation energies than round tubes and multiphase faceted nanotubes. The electronic properties of the defect-induced faceted PNTs are determined by the defect lines which control the band gap and the shape of the electronic states at the band edges. These band gaps increase with the radius of the nanotubes and converge to those of isolated defect lines.

DOI: 10.1103/PhysRevB.92.104104 PACS number(s): 61.46.Np, 71.20.Mq, 73.22.−f, 71.15.Mb

I. INTRODUCTION

Phosphorene, a single layer of phosphorus, was recently proposed and synthesized [1–4]. Its high mobility and tunable finite band gap, among other promising properties [5–9], make it an interesting new member of the ever increasing family of quasi-two-dimensional (2D) materials. The most well-known member of this family is graphene which consists of a 2D hexagonal lattice with two carbon atoms per unit cell. The resulting honeycomb structure, in which every atom forms covalent bonds with its three closest neighbors, forms the basic geometry of most other 2D materials, such as boron nitride and silicene. There are basically two ways in which the bonds with the three nearest neighbors are formed, namely through sp^2 and sp^3 hybridization of the atoms (or mixtures of the two). The atoms in graphene have sp^2 hybridization and this results in a strong network of in-plane σ bonds. On top of this, there is a π-bond network from the p_z orbitals which determines the electronic properties of graphene and turns it into a semimetal. In contrast to the C atoms of graphene, the P atoms in phosphorene have sp^3 hybridization. This is mainly caused by the extra valence electron of phosphorus in comparison to carbon. Indeed, if these extra electrons are placed in a sp^2-hybridized structure, they would occupy the energetically unfavorable (antibonding) π^* band. However, with sp^3 hybridization, a σ-bond network can be formed with three sp^3 orbitals and the other sp^3 orbital is used to host the remaining electron pair. This leads to an essentially tetragonal coordination of the P atoms and results in a buckled nature of sp^3-hybridized sheets. The out-of-plane positions of the atoms in sp^3-hybridized sheets give rise to various possible structural phases which are absent in sp^2-hybridized systems. In the case of phosphorene, this extra freedom leads to a plethora of structural phases [10,11] of which black (α-phase) and blue (β-phase) phosphorene (see Fig. 1) are the most stable ones.

Most 2D crystals, such as graphene and boron nitride, can also be used to create nanotubes by rolling up the sheets. Due to the buckled nature of the phosphorene family, the traditionally rolled-up nanotubes can be modified in various ways. As shown by Guan *et al.* [12], it is possible to join different structural phases of phosphorene to create so-called faceted nanotubes with lower formation energies than simple rolled nanotubes. These faceted tubes are made up of different phases that form well-defined angles when they are joined together. When a suitable combination of such structural phases is used, the structure can be closed to form a tube without inducing bending strain as in rolled nanotubes.

In the present work, we have taken a different approach to reduce the formation energy of phosphorene nanotubes (PNT). We start from (single-phase) blue phosphorene sheets and introduce various defect lines to induce kinks with well-defined angles in the system. Combining the defect lines in appropriate ways leads to faceted blue PNT with low formation energies. The advantage of this approach is that the energetically unfavorable phases are kept to a minimum. Here, we investigate the stability and electronic properties of these faceted tubes and compare them to the traditional rolled tubes and to the faceted multiphase tubes.

Our work is organized as follows: First we study rolled blue PNTs. Then we introduce various defect lines and calculate the corresponding formation energies and the angles of the resulting kinks. We use this information to create energetically interesting faceted PNTs in the next section. Finally, we investigate the electronic properties of the obtained structures and summarize our results.

II. COMPUTATIONAL DETAILS

Our first-principles calculations are based on density function theory as implemented in the Vienna *ab initio* Simulation Package (VASP) [13–16]. A plane-wave basis set and the projected augmented wave (PAW) method [17,18] are used to describe the wave functions. The cutoff energy of the basis is set to 500 eV and five electrons ($3s^2 3p^3$) of the phosphorus atom are treated as valence electrons. Exchange-correlation interactions are treated with the generalized

[*]yierpan.aierken@uantwerpen.be
[†]ortwin.leenaerts@uantwerpen.be
[‡]francois.peeters@uantwerpen.be

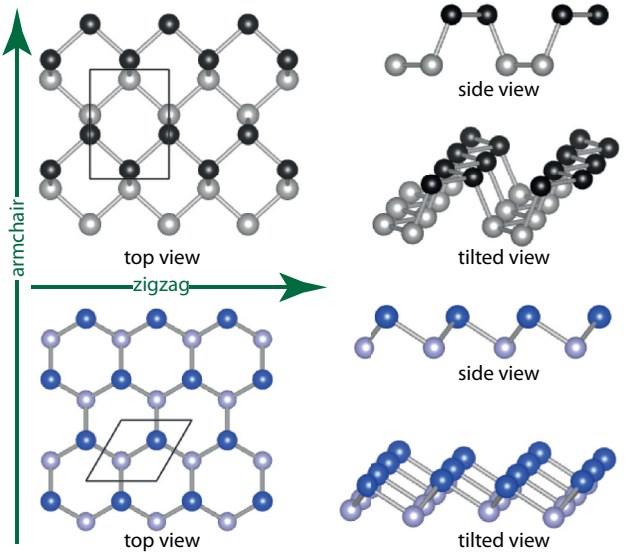

FIG. 1. (Color online) Monolayer structures of black (first row) and blue (second row) phosphorenes. Atoms are colored according to the names of the allotropes, and are lighter in color for the bottom layer of the buckled structure. The black boxes indicate the unit cell of each structure.

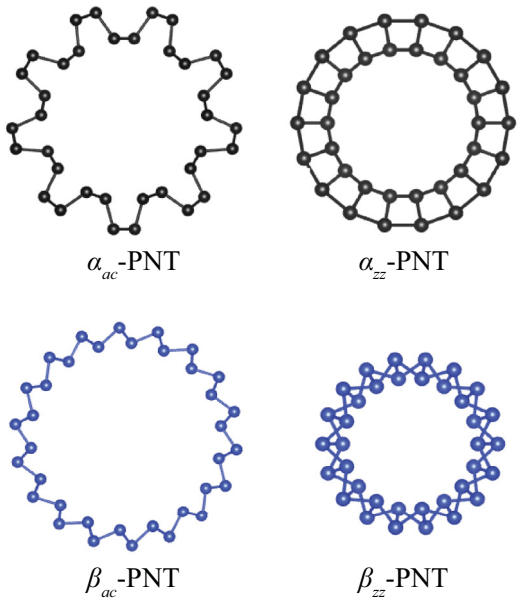

FIG. 2. (Color online) Rolled structures of α-PNT and β-PNT seen from the axial direction. The subscripts indicate the directions of the chiral vector, i.e., *ac* for armchair and *zz* for zigzag.

gradient approximation (GGA) within the Perdew-Burke-Ernzerhof (PBE) formulation [19,20]. A $15\times15\times1$ k-point mesh is used to sample the Brillouin zone for monolayer structures and a $1\times1\times15$ grid is used for nanotube structures. A vacuum space of 15 Å is incorporated to avoid interlayer and intertube interactions in monolayer and nanotube calculations, respectively. The energy convergence criterion for the self-consistent calculations is set to 10^{-5} eV, while the force convergence criterion for the ionic steps is set to 10^{-3} eV/Å.

III. RESULTS

A. Rolled phosphorene nanotubes

As a reference, we first investigate the rolled α-PNT and β-PNT that result from rolling up black and blue phosphorene sheets, respectively. A cross section of the structure of some typical examples is shown in Fig. 2. In principle, there is an infinite number of possible tubes but we restrict our study to the chiral tubes rolled up along the armchair and zigzag directions. Such PNTs were also studied previously [12,21] and our results compare well with those recent calculations as shown below. For large tubes, the formation energy of the tubes can be mainly attributed to the strain energy that results from bending the phosphorene sheets. It has been demonstrated with a simple continuum elastic model that the bending energy follows a R^{-2} dependence, in which R denotes the radius of the nanotube [22,23]. Deviations from this ideal behavior can be expected for small tubes where the finite thickness of the phosphorene sheet and the interatomic interactions between non-nearest neighbors become important.

We calculated the strain energy for armchair and zigzag nanotubes of α-PNT and β-PNT as a function of their radii show the results in Fig. 3 together with the results of Refs. [12,21]. The strain energy is here defined as the energy difference per P atom between the rolled PNT and a corresponding phosphorene sheet, i.e., $E_S^x = (E_{\rm PNT}^x - E_{\rm sheet}^x)/N$, in which N denotes the number of atoms and $x = \alpha,\beta$. Since the strain energy of ideal nanotubes follows a R^{-2} law, we try to fit our data by a power law of the form $E_S = aR^{-b}$. In Table I, we show the coefficients of this fitting function for all the different nanotubes. It is clear that the strain energy of the rolled PNT approximately follows the inverse-square law based on the bending energy. Note, however, that a substantial deviation from this trend is observed for zigzag nanotubes made of black phosphorene. This can be attributed to the large buckling in the transverse direction which effectively increases the thickness of the bended sheet. Another interesting observation is that the blue phosphorene phase becomes more stable than black

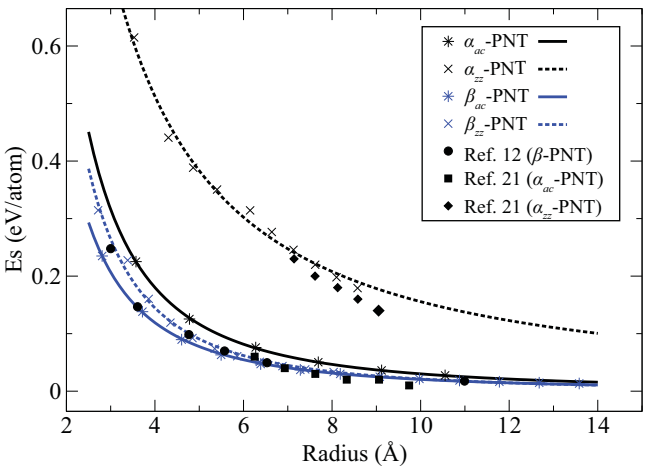

FIG. 3. (Color online) Strain energy versus radius of rolled nanotubes. The curves correspond to aR^{-b} fits, where the fitting parameters are listed in Table I.

TABLE I. Fitting coefficients for the strain energy $E_S = aR^{-b}$ of rolled PNTs shown in Fig. 3.

	α_{zz}-PNT	α_{ac}-PNT	β_{zz}-PNT	β_{ac}-PNT
a	3.11	2.70	2.63	1.70
b	1.30	1.95	2.09	1.92

phosphorene for small nanotubes: The cohesive energy of 2D black phosphorene sheets is about 10 meV/atom larger than that of blue phosphorene [10] and this is easily compensated by the reduced bending energy of blue phosphorene.

The strain energy of all the round nanotubes increases rapidly as the tube radius decreases. At some point the strain energy might become so large that it is more favorable to alter the structure in order to release some of the built-up energy. As discussed in the introduction, Guan *et al.* [10] showed that specific partial structural phase transitions can lead to substantial energy gains. As a result, the PNTs loose their round character and acquire a faceted appearance. The different facets of the tube consist of nearly flat phosphorene nanoribbons with well-defined structural phases that are glued together at almost no expense. The structural phase transitions raise the energy, but this is more than compensated by the reduced strain energy for small PNTs.

B. Defect lines

In our work, we take another approach to release the strain energy. In contrast to the faceted tubes of Guan *et al.* [12] that contain considerable large parts with unfavorable structural phases, we try to maximize the amount of the low-energy blue phosphorene (β phase) in the nanotubes. This can be done by the introduction of defect lines that create kinks in the phosphorene sheet. We will use the β phase for this purpose for two different reasons: (i) as discussed above, the β phase has lower energy for small tubes, and (ii) it is easier to introduce defect lines in the β phase than in the α phase (black phosphorene). The β phase consists of P atoms that are alternately shifted up and down with respect to the crystal plane [i.e., one sublattice (A) buckles up, while the other (B) buckles down]. Defect lines are created by breaking this ordered pattern along one-dimensional (1D) lines, which can be done in several ways. We restrict our study to lines in the zigzag and armchair directions in order to create armchair and zigzag nanotubes, respectively. Three types of defect lines, C, D, and F, in the zigzag direction are considered and two, G and H, in the armchair direction. The structure of these defect lines is depicted in Fig. 4 and we give their formation energies in Table II. The defect lines induce kinks in the phosphorene sheets and the angle of these kinks is also given in Table II. The formation energy of a defect line is defined as $E_f^l = (E_{\text{defect}} - E_{\text{sheet}})/L$ in which L is the length of the defect line. Practically, this property can be calculated in a system that combines two defects of the same kind but with opposite orientation (i.e., angle) in a periodic structure, as illustrated in Fig. 4. The following nomenclature will be applied in order to distinguish between the different defects: Superscripts (ac or zz) are used to indicate the type of tubes that are produced by the defects (armchair or zigzag); subscripts (AA, AB, BA, and BB) correspond to the buckling on the two sides of the defect line, A (B) meaning sublattice A up and B down (B up and A down).

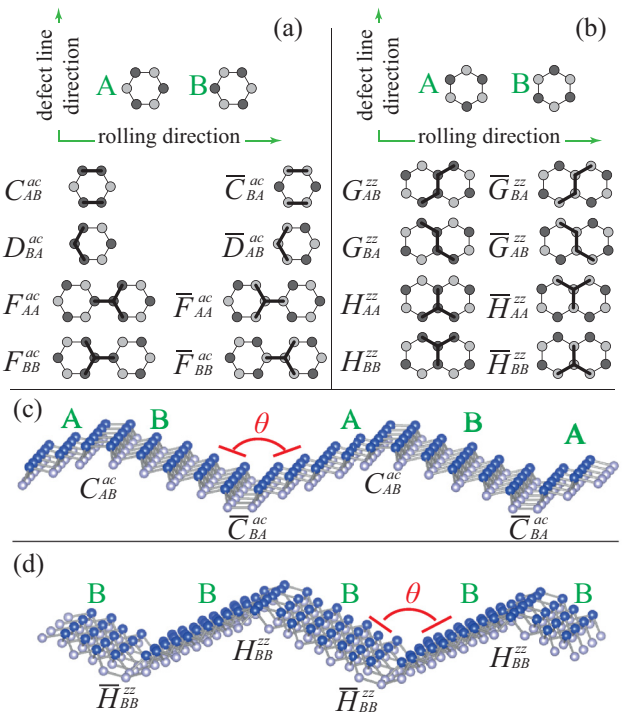

FIG. 4. (Color online) Different types of defect for (a) armchair and (b) zigzag directions. The dark and light shaded atoms indicate that they are buckled up or down, respectively. Effective location of the defect is represented by a thick black line. Overlined defect name refer to the same defect but with an opposite opening direction of the angle. (c) and (d) Tilted view of the C and H defect lines incorporated in the β phase.

Note that one can distinguish two kinds of defects: (i) defects that leave the β phase unaltered on both sides of the defect line and (ii) those defects that invert the buckling orientation on one side with respect to the other. $F^{ac}_{AA/BB}$ and $H^{zz}_{AA/BB}$ belong to the first type, while C^{ac}_{AB}, D^{ac}_{BA}, and $G^{zz}_{AB/BA}$ belong to the second type.

C. Defect-induced faceted PNTs

The different defect lines discussed above can now be combined to create defect-induced faceted PNTs (DIF-PNTs). According to the type, the formation energy, and the preferred angles of the defects, we can make intuitive guesses about which defect combinations are possible and energetically favorable. Some examples of DIF-PNTs are pictured in Fig. 5.

TABLE II. The formation energy E_f^l, the and kink angle θ of the different defect lines that are illustrated in Fig. 4.

	C^{ac}	D^{ac}	F^{ac}	G^{zz}	H^{zz}
E_f^l(eV/Å)	0.0493	−0.0017	0.0747	0.0872	0.1918
θ (°)	139.711	112.453	89.531	118.549	126.706
E_{gap} (eV)	1.56	1.64	1.43	1.28	1.20

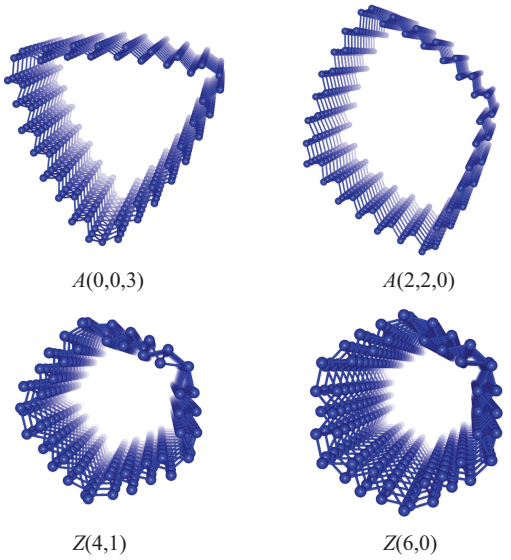

FIG. 5. (Color online) Selected examples of defect-induced faceted PNTs.

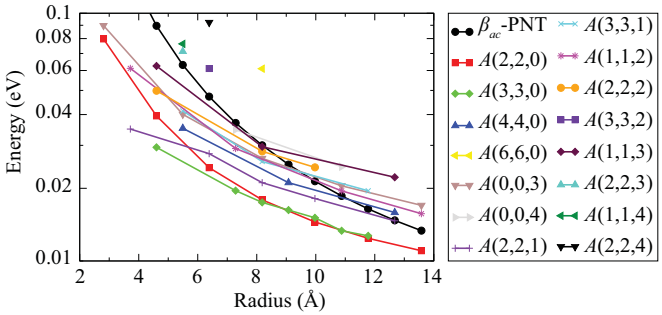

FIG. 6. (Color online) The formation energy E_f^t of armchair DIF-PNTs compared with the strain energy E_S^β of β_{ac}-PNT (black curve with circle symbols).

Not all defect combinations are possible or favorable and we therefore used the following guidelines to make potentially interesting tubes: (i) An even number of defects that invert the buckling (i.e., the second type of defects discussed in the previous section) must be included to make closed nanotubes. (ii) The total number of defects should be as small as possible because every defect line has a finite formation energy. (iii) For a nanotube with N defects, the sum of the defect angles should be close to $(N-2)\times 180^\circ$ in order to avoid straining the angles too much.

To compare the DIF-PNTs with round tubes, we need to define some radius for the faceted tubes. To this end, we use the radius of a rolled tube with the same orientation and number of P atoms as the DIF-PNT. The radius of the DIF-PNTs is not only determined by present defect lines, but also by the size of the defect-free β-phase regions which can also be varied. The formation energy of the DIF-PNT is defined as $E_f^t = (E_{\text{DIF-PNT}} - E_{\text{sheet}})/N$, where N is the number of atoms. When the angles are perfectly matched in some ideal faceted tube, the formation energy of the tube is expected to decrease as R^{-1} instead of the R^{-2} dependence of round tubes. This R^{-1} dependence simply follows from the fact that the formation energy of the defects is (nearly) independent of the radius, while the number of atoms increases linearly with the size of the radius of the tube. The different behavior of the formation energies of (ideal) faceted and round nanotubes as a function of radius implies that there will be a crossover radius R_0 such that faceted tubes with $R < R_0$ are more stable than round ones.

We will first take a look at armchair PNTs and consider zigzag PNTs in the next section.

Armchair PNTs. For armchair nanotubes, we need defect lines along the zigzag direction. We discussed three of such defects above and we will combine them to make energetically favorable armchair DIF-PNTs. The first two defects, C_{AB}^{ac} and D_{BA}^{ac}, have opposite effects on the buckling of the P atoms and should always appear in pairs in order to match the buckling at the two edges of the nanoribbon. The third defect, $F_{AA/BB}^{ac}$, can be regarded as a combination of the first two and can always be added to an existing tube. In order to distinguish the different defected nanotubes we introduce the notation $A(m,m,n)$ to indicate an armchair (A) DIF-PNT with m defects of the first and second kind and n of the third. To keep the strain on the defect angles low, we need at least three defects (triangular tube).

The only possibilities for such tubes are $A(1,1,1)$ and $A(0,0,3)$. The strain on the first one is considerable and this kind of tube is therefore not considered. Quadrilateral tubes can be made from the following combinations: $A(2,2,0)$, $A(1,1,2)$, and $A(0,0,4)$. Pentagons and hexagons can be formed with $A(2,2,1)$, $A(1,1,3)$, $A(0,0,5)$, $A(3,3,0)$, $A(2,2,2)$, $A(1,1,4)$, and $A(0,0,6)$. The third and seventh type of tubes are not considered because of the excessive incorporation of the most energetically unfavorable F^{ac} defects. Adding more defect lines becomes unfavorable because in this case large tubes are required to incorporate such number of defects. Therefore, we only investigate the smallest possible nanotubes as typical examples and do not consider their behavior as a function of the tube radius. All the different combinations that were used are depicted in Supplemental Material [24].

In Fig. 6, the formation energy of the different armchair PNTs is shown as a function of tube radius for both faceted and round tubes. The crossover in the formation energy between the faceted and round tubes is nicely observed for several faceted nanotubes such as $A(0,0,3)$. The point where the crossover occurs depends on the type and number of defects and ranges from approximately 7 Å to more than 15 Å. The most favorable armchair DIF-PNTs are the quadrilateral $A(2,2,0)$ and the hexagonal $A(3,3,0)$ nanotubes with a slight preference for the latter. Due to their larger formation energy, F^{zz} defects are rarely included in the energetically favorable armchair DIF-PNTs.

Zigzag PNTs. For zigzag nanotubes, only two kinds of defect lines are included to make faceted tubes, namely G^{zz} and H^{zz}. We use the notation $Z(m,n)$ to indicate a zigzag (Z) DIF-PNT with m defects of the first and n of the second kind; see Fig. 5 for examples. The total number of G^{zz} defects should be even, while the number of H^{zz} defects is arbitrary. Again, we need at least three defect lines and the only possibility is $Z(0,3)$ in this case. Quadrilateral tubes can be made from $Z(4,0)$, $Z(2,2)$, and $Z(0,4)$. Other tubes that we considered

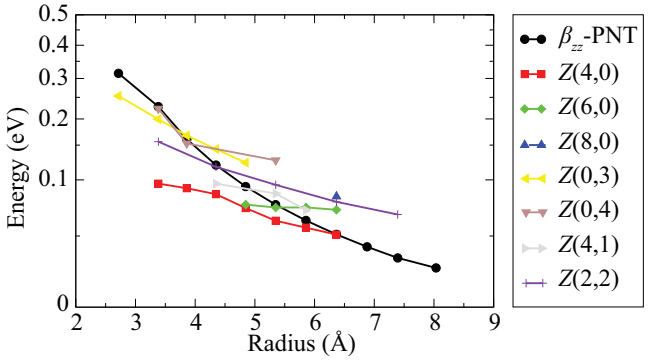

FIG. 7. (Color online) The formation energy E_f^t of zigzag DIF-PNTs compared with the strain energy E_S^β of β_{zz}-PNT (black curve with circle symbols).

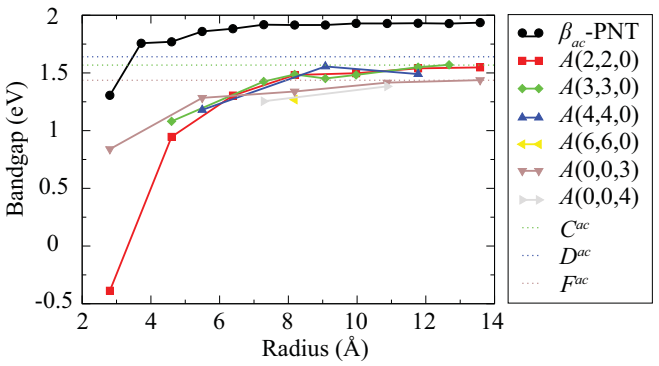

FIG. 8. (Color online) Armchair DIF-PNTs band gaps compared with rolled β_{ac}-PNT (black curve with circle symbols).

are $Z(4,1)$, $Z(6,0)$, and $Z(8,0)$. All the different combinations that were used are depicted in Supplemental Material [24].

In Fig. 7, the formation energy of the different zigzag PNTs is shown as a function of tube radius for both faceted and round tubes. It is seen that the crossover in the formation energy between the faceted and round tubes also occurs for the zigzag nanotube, but at much smaller radii as compared to the armchair nanotubes (from approximately 4 to 6.5 Å). The quadrilateral $Z(4,0)$ tubes are found to be the most stable zigzag DIF-PNTs.

It is interesting to examine the formation energy of the faceted armchair and zigzag PNTs in more detail. We can fit the formation energy of the different tubes with the function $E_f^t = aR^{-b}$. This function has the same form as the strain energy (E_S) defined in Sec. III A, but it now includes both strain energy and defect energy. A b parameter close to 2 indicates that the strain energy dominates in the system, while $b \approx 1$ is expected for nonstrained defected tubes. In Table III, we give the fitting parameters as obtained for some typical types of DIF-PNT. The round tubes (β_{ac}-PNT and β_{zz}-PNT) have indeed parameters close to 2 and the defected tubes have fitting parameters close to 1, although there are some substantial deviations in the case of faceted zigzag nanotubes because of the limited number of data points and the smallness of the tubes.

IV. ELECTRONIC PROPERTIES

In the next section, we will investigate the electronic properties of the DIF-PNTs with a focus on the electronic band gap. In contrast to the inverse proportionality of the band gap with diameter in carbon nanotubes [25], the band gap of round PNTs increases with the size of the radius. For multiphase faceted PNTs, it was shown previously that the band gap does not show any clear dependence on the radius but rather spans the range between the composing structural phases [12].

In Fig. 8 we show the band gaps of the armchair DIF-PNTs together with the results for the rolled β_{ac}-PNT. A clear dependence of the band gap on the radius can be observed. The band gap increases with radius and converges to two different limits, well below the limit of the round tubes. The origin of this behavior lies in the character of the valence band maximum (VBM) and conduction band minimum (CBM) states of the DIF-PNTs which determine the size of the band gap. As illustrated in the insets of Fig. 9, the VBM and CBM states are localized on the defect lines. In other words, the defect levels associated with the defect lines fall inside the blue phosphorene

TABLE III. Fitting coefficients for the formation energy $E_f^t = aR^{-b}$ of DIF-PNTs.

	β_{ac}-PNT	$A(2,2,0)$	$A(3,3,0)$	$A(0,0,3)$	$A(0,0,4)$	$A(2,2,1)$	$A(3,3,1)$
a	1.70	0.33	0.12	0.28	0.19	0.16	0.24
b	1.92	1.37	0.89	1.12	0.86	0.93	1.04
	β_{zz}-PNT	$Z(4,0)$	$Z(6,0)$	$Z(0,3)$	$Z(0,4)$	$Z(4,1)$	
a	2.63	0.61	0.30	0.87	0.34	3.70	
b	2.09	1.36	0.88	1.23	0.59	2.25	

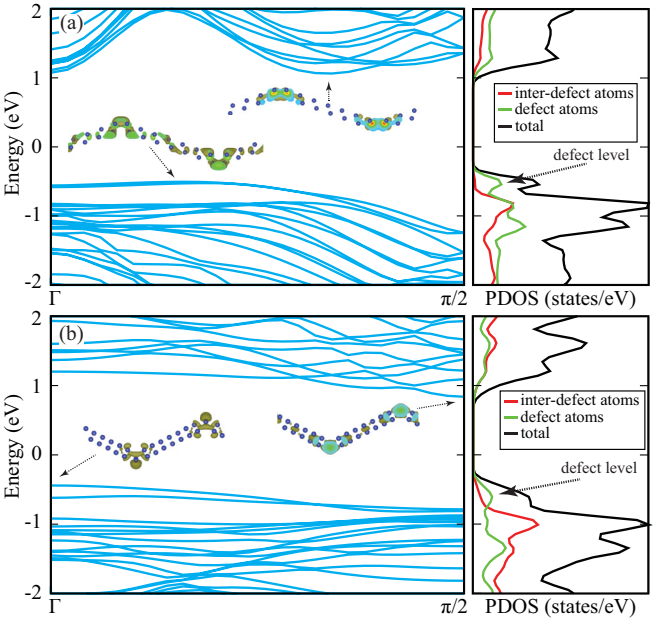

FIG. 9. (Color online) Band structure (along defect line) and PDOS of selected DIF-PNTs, (a) for C^{av} and (b) for G^{zz}. (Insets) Charge density at CBM and VBM.

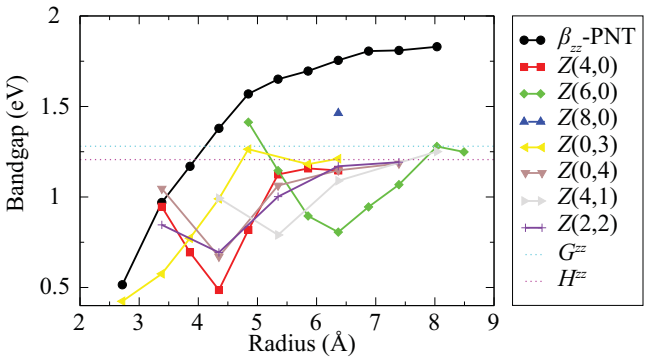

FIG. 10. (Color online) Zigzag DIF-PNTs band gaps compared with rolled β_{zz}-PNT (black curve with circle symbols).

gap and determine the band gap of the defect-induced faceted PNTs. This is confirmed by the partial density of states (PDOS) in Fig. 9, where a clear defect peak in the PDOS can be found inside the band gap of pure (inter-defect) blue phosphorene. Therefore, the electronic band gap will not converge to the blue phosphorene limit, but rather to the gap size of the isolated defects as calculated in Sec. III B (Table II). The tubes contain various types of defects, but the defect with the smallest gap determines the total band gap of the tube. The decreased band gaps for smaller tubes can be attributed to inter-defect interactions and possibly to some remaining bending stresses. The decrease in the band gap when the distance between the defect lines decreases was also observed for the defected phosphorene sheets, illustrated in Fig. 4, in which no bending strain was present.

The dependence of the band gap on the radius of the zigzag DIF-PNTs is shown in Fig. 10. As for the zigzag DIF-PNTs, the band gaps converge to that of the isolated defects for large radii. When compared to armchair DIF-PNTs, a different behavior can be observed for tubes with small radii: With decreasing radius the band gap first decreases, but then it increases again for very small radii. The first decrease can be attributed to the interaction between the different defect states. The increase of the band gap for very small radii might be attributed to the structural interaction between the defects: The defects of the zigzag nanotubes are wider (i.e., they distort the blue phosphorene phase over a wider range) than the armchair ones and become structurally distorted when the distance between them becomes smaller.

A. Comparison to multiphase faceted PNT

In the last part of this work, we will compare our results of DIF-PNTs to the multiphase faceted PNTs proposed by Guan *et al.* [12]. These last tubes are made of fixed combinations of α, β, γ, and δ-phase phosphorene with variable widths, as depicted in Fig. 1 of Ref. [12]. Our most favorable armchair DIF-PNTs, namely the $A(3,3,0)$ tubes, are closely related to some of the tubes of Guan *et al.* and have similar symmetry and formation energies. The (nearly) equally stable quadrilateral $A(2,2,0)$ tubes, on the other hand, fall outside their description due to the different number of facets. The DIF-PNTs are not restricted to the triangular symmetry of the multiphase PNTs and allow therefore for a much larger variety of possible low-energy nanotubes.

For zigzag PNTs the differences are even larger. Our zigzag DIF-PNTs have no analogs in the multiphase description because the multiphase zigzag PNTs are exclusively built from the energetically less favorable γ and δ phases. The multiphase description provides only one structure with lower formation energy than rolled β-PNT [see Fig. 3(a) of Ref. [12]], in contrast to the multitude of zigzag DIF-PNTs with lower formation energies that we found (see Fig. 7). Blue (β) phosphorene is significantly better suited to make small zigzag PNTs than the other structural phases (α, γ, and δ).

V. SUMMARY AND CONCLUSIONS

In this work, we investigated a new class of faceted phosphorene nanotubes using first-principles calculations. We started our study by examining round armchair and zigzag PNTs of black and blue phosphorous and showed that blue phosphorene is better suited to make small nanotubes. Then we proposed five different types of defect lines to create kinks in β-phosphorene sheets. We investigated the formation energy and kink angle of these defects and used this information to create defect-induced faceted PNTs. After identifying some suitable defect combinations, we calculated the formation energy as a function of the PNT radius and demonstrated the enhanced stability of the DIF-PNTs with respect to round tubes. We showed that the VBM and CBM states of the DIF-PNTs are localized on the defect lines and that these states control the electronic properties of the tubes. The band gap of armchair DIF-PNTs increases with the radius and converges to the gap corresponding to isolated (infinitely separated) defect lines. For zigzag DIF-PNTs, a more complicated behavior was observed which originates from the wider structural distortions associated with the defect lines.

Finally, we compared our defect-induced PNTs with the multiphase faceted PNTs proposed by Guan *et al.* [12]. We found similar formation energies for armchair PNTs, but more favorable DIF-PNTs can be created with small radii due to less stringent restrictions regarding the structure (symmetry) of the tubes. For zigzag PNTs, the DIF-PNTs are significantly more stable in comparison to rolled β-PNTs and previously reported multiphase faceted PNTs. Furthermore, we found a much larger variety of stable zigzag PNTs.

ACKNOWLEDGMENTS

This work was supported by the Fonds Wetenschappelijk Onderzoek (FWO-Vl). The computational resources and services used in this work were provided by the VSC (Flemish Supercomputer Center), funded by the Hercules Foundation and the Flemish Government, department EWI.

[1] L. Li, Y. Yu, G. J. Ye, Q. Ge, X. Ou, H. Wu, D. Feng, X. H. Chen, and Y. Zhang, Nat. Nanotech. **9**, 372 (2014).

[2] H. Liu, A. T. Neal, Z. Zhu, Z. Luo, X. Xu, D. Tománek, and P. D. Ye, ACS Nano **8**, 4033 (2014).

[3] S. P. Koenig, R. A. Doganov, H. Schmidt, A. H. Castro Neto, and B. Özyilmaz, Appl. Phys. Lett. **104**, 103106 (2014).
[4] W. Lu, H. Nan, J. Hong, Y. Chen, C. Zhu, Z. Liang, X. Ma, Z. Ni, C. Jin, and Z. Zhang, Nano Res. **7**, 853 (2014).
[5] A. Jain and A. J. H. McGaughey, Sci. Rep. **5**, 8501 (2015).
[6] Q. Wei and X. Peng, Appl. Phys. Lett. **104**, 251915 (2014).
[7] L. Kou, T. Frauenheim, and C. Chen, J. Phys. Chem. Lett. **5**, 2675 (2014).
[8] M. Tahir, P. Vasilopoulos, and F. M. Peeters, Phys. Rev. B **92**, 045420 (2015).
[9] X. Y. Zhou, R. Zhang, J. P. Sun, Y. L. Zou, D. Zhang, W. K. Lou, F. Cheng, G. H. Zhou, F. Zhai, and K. Chang, Sci. Rep. **5**, 12295 (2015).
[10] J. Guan, Z. Zhu, and D. Tománek, Phys. Rev. Lett. **113**, 046804 (2014).
[11] M. Wu, H. Fu, L. Zhou, K. Yao, and X. C. Zeng, Nano Lett. **15**, 3557 (2015).
[12] J. Guan, Z. Zhu, and D. Tománek, Phys. Rev. Lett. **113**, 226801 (2014).
[13] G. Kresse and J. Hafner, Phys. Rev. B **47**, 558 (1993).
[14] G. Kresse and J. Hafner, Phys. Rev. B **49**, 14251 (1994).
[15] G. Kresse and J. Furthmüller, Comput. Mater. Sci. **6**, 15 (1996).
[16] G. Kresse and J. Furthmüller, Phys. Rev. B **54**, 11169 (1996).
[17] P. E. Blöchl, Phys. Rev. B **50**, 17953 (1994).
[18] G. Kresse and D. Joubert, Phys. Rev. B **59**, 1758 (1999).
[19] J. P. Perdew, K. Burke, and M. Ernzerhof, Phys. Rev. Lett. **77**, 3865 (1996).
[20] J. P. Perdew, K. Burke, and M. Ernzerhof, Phys. Rev. Lett. **78**, 1396 (1997).
[21] H. Guo, N. Lu, J. Dai, X. Wu, and X. C. Zeng, J. Phys. Chem. C **118**, 14051 (2014).
[22] G. G. Tibbetts, J. Cryst. Growth **66**, 632 (1984).
[23] D. H. Robertson, D. W. Brenner, and J. W. Mintmire, Phys. Rev. B **45**, 12592 (1992).
[24] See Supplemental Material at http://link.aps.org/supplemental/10.1103/PhysRevB.92.104104 for the different armchair and zigzag DIF-PNTs that were used in the calculations.
[25] T. W. Odom, J.-L. Huang, P. Kim, and C. M. Lieber, J. Phys. Chem. B **104**, 2794 (2000).